Article citation info:
Mattallah S, Kelaiaia R, Louahem M'Sabah H, Kerboua A. Application of artificial neural networks for the prediction of the service conditions of an elastohydrodynamic EHL contact in the presence of solid pollutant. Diagnostyka. 2024;25(1):2024107. https://doi.org/10.29354/diag/178317.



**DIAGNOSTYKA**, 2024, Vol. 25, No. 1

**e-ISSN** 2449-5220
**DOI:** 10.29354/diag/178317

# APPLICATION OF ARTIFICIAL NEURAL NETWORKS FOR THE PREDICTION OF THE SERVICE CONDITIONS OF AN ELASTOHYDRODYNAMIC EHL CONTACT IN THE PRESENCE OF SOLID POLLUTANT

**Sabrina MATTALLAH [1, 2, *], Ridha KELAIAIA [1, 2], Hanane LOUAHEM M'SABAH [2], Adlen KERBOUA [3]**

[1] Laboratory of Mechanical Engineering and Materials, University of August 20, 1955- Skikda, Algeria
[2] Department of Mechanical Engineering, University of August 20, 1955-Skikda, Algeria
[3] Department of Petrochemical, University of August 20, 1955-Skikda, Algeria
[*] Corresponding author, e-mail: s.mattallah@univ-skikda.dz

Abstract

Lubricated mechanical mechanisms operate under service conditions influenced by several environmental parameters, and their lifetimes may be threatened due to inappropriate use or by the presence of solid contaminants. The objective of this work is to study the effect of three operating parameters, namely: rotational speed $V$, load $Q$ and kinematic viscosity $\nu$ in the presence of three sizes of solid contaminants $T$, on the degradation of an EHL contact, to predict the ranges of effects that may lead to the damage of the contacting surfaces. In our investigation, an experimental design of nine trials is used to combine four factors with three levels each to accomplish the experimental investigation. Artificial neural network regression and the desirability function were used for the interpretation and modelling of the responses, which are: wear $W$, arithmetic mean height $Ra$, total profile height $Rt$ and maximum profile height $Rz$. From these methods we observed that the sand grain sizes have a significant impact on the wear $W$ and the roughness $Ra$, but that viscosity has the primary influence on the variation of the roughnesses $Rt$ and $Rz$. We also found that the quality of the predicted models is very good, with overall determination coefficients of $R^2$ learning = 0.9985 and $R^2$ validation = 0.9996. Several levels of degradation depending on the operating conditions are predicted using the desirability function.

Keywords: elastohydrodynamic contact, solid pollution, artificial neural network, wear.

**List of Symbols/Acronyms**

$(\mu m)$– Solid contaminants;
$\overline{y_i}$ – Average response;
$\widehat{y_i}$– Predicted response;
$\sigma\overline{y_i}^2$– Uncertainty;
$R^2$ – The coefficient of determination;
$W_i$ – The weight;
$y_i$ – Experiment response;
$b_i$ – the bias;
D– The desirability;
Xi – Input vector;
$\sigma(y)$ – Standard deviation;
$MAD$ – The Mean Absolute Deviation;
$Q\ (N)$– Load;
$RMSE$ – The Root Mean Square Error;
$Ra$ – Arithmetic mean height [µm];
$Rt$ – Total profile height [µm];
$Rz$ – Maximum profile height [µm];
$V\ (rpm)$– Rotational speed
$W$ – Wear [mm];
$di$– The individual desirability;
$\nu\ (cSt)$– Kinematic viscosity;

## 1. INTRODUCTION

Mechanical contacts affected by solid pollution can undergo accelerated degradation and many studies have been conducted in this context to try to predict the degree of early degradation. Several contributions from researchers have studied the behaviour of the elastohydrodynamic contact, including [1], which briefly reviews the history of its development, and [2], which highlights the progress that has been made since then, both in numerical modelling and in experimental research on EHL. Several papers address the lubrication performance and the mechanisms that govern EHL film formation [3-8]. The authors of [9] clarify the relevant aspect of the viscosity–temperature–pressure relationship of lubricating oils. Ultrasound is also used by [10] to determine the thickness of the oil film in elastohydrodynamically lubricated (EHL) contacts for opposing surfaces completely separated by the liquid layer. The effects of different rough

Received 2023-05-22; Accepted 2024-01-06; Available online 2024-01-09

topographies combined with the associated particle parameters on EHL performance and the minimum film thickness distribution under different loads, operating speeds and initial viscosities are also studied by [11]. In [12], the authors have addressed the combination of elastohydrodynamic lubrication (EHL) and the inclusion problem to consider the effect of material inhomogeneity on the lubrication performance and subsurface stress distribution. On the other hand, the elastic deformation of the interface greatly influences the overall performance of the oil film, which is related to the material, inlet pressure, velocity, viscosity and the minimum oil film thickness that determines the LHS [13]. The roughness of the surfaces in lubricated contact is studied in turn in order to deduce the disturbance of the lubricating film thickness [14-18], and also in this axis [19] reports new updated film parameter, which takes into account the elastohydrodynamic lubrication effects induced by surface irregularities at the microscopic scale (micro-EHL). The consequences of particle entrapment have been analysed theoretically and experimentally in numerous works [20-23], and extensive research has been carried out on surface indentation, wear, scratching, frictional heating, acoustic emission (noise), scratching and overall reduction in the remaining life of contacts.

The study of the influence of the service parameters of EHL contacts and their interactions on the functioning of the mechanisms requires the introduction of experimental designs and statistical methods. Several methods are used, such as regression based on parametric functions [24-25].

This paper presents an original investigation based on artificial neural networks that uses non-parametric functions for regression. In order to predict the degradation of the EHL contact, a study of the influence of the parameters: rotation speed, load and kinematic viscosity in the presence of three sizes of solid pollutant is carried out. This work allows us to test the simultaneous variation of the parameters studied.

## 2 EXPERIMENTAL DEVICE AND EQUIPMENT USED

This work is a study that tests parameters for which well-defined value levels are imposed. The design of experiments is a tool that allows a large number of parameters to be tested with a reduced number of tests on a single sample. The tests are carried out at a temperature and pressure that do not affect the progress of the tests.

The test device [25] is configured in such a way that the experiments can be carried out without any problems. In fact, a rotating steel disc and a cylindrical specimen are mounted in contact, nine strips are used for friction and the tenth is a witness strip as shown in Fig. 1, and the duration of each test is 20 min in the device.

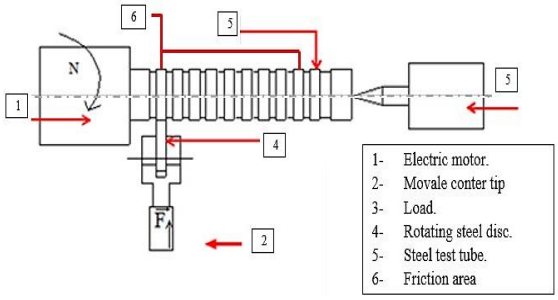


Fig. 1. Schematic of the test set-up used

The equipment used to carry out the experiments was a cylindrical test tube made of 316L stainless steel, Ø50 mm and 240 mm long. The test piece consists of nine strips, separated from each other by small grooves 2 mm deep; stainless steel discs 316 L, Ø50; fillers; and sand filtered to 63, 90 and 125 microns with a concentration of 5 g/l in the lubricant used. A digital caliper was used to measure the loss of ribs; a roughness meter to measure the roughness; and three types of oil (as listed in Table 1).

The experimental design used in this investigation is a Taguchi L9 design with 4 factors and 3 levels each, namely: $T$ (particle sizes ($\mu m$)); $Q$ (load ($N$)); $V$ (rotation speed ($rpm$)); and $\nu$ (kinematic viscosity ($cSt$)) as shown in Table 2. This choice allows a minimum of tests and a reduced blow.

Table 1. Viscosity classification of oils

| **Viscosity classes** | **Kinematic viscosity limits (cSt) at 40°C** |
|---|---|
| ATF II D | 36 à 40 |
| ISO VG 150 | 135 à 165 |
| ISO VG 220 | 198 à 242 |

Table 2. Levels of factors in the experiment series

| **Viscosity $\nu$ ($cst$)** | **Rotation speed $V$ ($rpm$)** | **Size of particles $T$ ($\mu m$)** | **Loading $Q$ ($N$)** |
|---|---|---|---|
| 40 | 400 | 60 | 100 |
| 150 | 1000 | 90 | 130 |
| 220 | 1600 | 120 | 160 |

The parameters are chosen to simulate various conditions affecting the elastohydrodynamic contact, namely lubrication and contamination of the contact by various sizes of solid contaminants, as well as rotational speed and load, in order to predict the levels of operating parameters that will minimize degradation of the mechanical contact.

### 2.1. Checking response measurements

Measurement uncertainty can be caused by:

- Systematic errors,
- Accidental errors,
- Statistical dispersions

It is also well known that experimental tests give different results each time they are repeated, and the

propagation of uncertainties influences the quality of the investigations and creates difficulty when verifying the measured values. In our case, we carried out five measurements for each output, namely: wear w, roughness Ra, Rt, and Rz. For each parameter, we have nine tests, so 36 values to check and estimate their uncertainties (Table 3).

Table 3. Summary of wear and roughness measurement uncertainty Ra, Rt and Rz

| $\sigma\bar{Y}^2$W | $\sigma\bar{Y}^2$Ra | $\sigma\bar{Y}^2$Rt | $\sigma\bar{Y}^2$Rz |
|---|---|---|---|
| 0.005 | 0.001 | 0.0009 | 0.002 |
| 0.002 | 0.007 | 0.007 | 0.003 |
| 0.003 | 0.002 | 0.008 | 0.002 |
| 0.004 | 0.003 | 0.0009 | 0.002 |
| 0.004 | 0.005 | 0.006 | 0.009 |
| 0.008 | 0.005 | 0.007 | 0.002 |
| 0.004 | 0.003 | 0.002 | 0.005 |
| 0.008 | 0.001 | 0.002 | 0.007 |
| 0.006 | 0.005 | 0.004 | 0.008 |

By calculating the average of the five measurements, the absolute error $\sigma(y)$ (standard deviation) and the uncertainty $\sigma\bar{y}^2$ are given by the following formulae:

The average of the measurements is:

$$\bar{y} = \sum_{i=1}^{n} \frac{y_i}{n} \quad (1)$$

The experimental standard deviation given by the expression is: $\boldsymbol{\sigma}(Y) = \sqrt{\frac{1}{n-1}\sum_{i=1}^{n}(y_i - \bar{y}_i)^2}$ (2)

Uncertainty: $\sigma\bar{y}_i^{\,2} = \frac{1}{n}\,\sigma y^2$ (3)

The measurement result is written as follows: $\bar{y} \mp \sigma\bar{y}^2$

## 3 METHODOLOGIES

In order to exploit the results obtained, an artificial neural network method is used. The latter model complex relationships and can be used in regression, which is the case of our study. The network used (Fig. 2) has two hidden layers and a hyperbolic tangent activation function as fellow:

$$W_2 = f(W_1 * X + b_1) \quad (4)$$

$$f(x) = tanh(x) = \frac{e^x - e^{-x}}{e^x + e^{-x}} \quad (5)$$

$$y = W_2 * A + b_2 \quad (6)$$

Here, $W_2$ is the intermediate value between the two hidden layers, $X$ is input vector with four elements, then, we have three neurons in the first hidden layer, the weight matrix $W_1$ is a 3×4 matrix, the bias $b_1$ is also three elements vector.

In the second hidden layer, we have four neurons, the weight matrix $W_2$ is a 4×3 matrix, the bias $b_2$ and the output vector $y$ as four element vectors.

Where:

$$y = \begin{bmatrix} W \\ Ra \\ Rt \\ Rz \end{bmatrix}$$

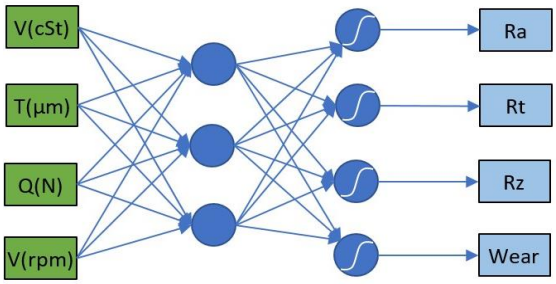


Fig. 2. Neural network used with a hidden layer

The objective is to prove that the model generates good estimates of the values of the variables under study. The training data is used to calibrate the model, while the validation set is used to show that the model is reliable and relevant.

Once the model has been created with the training dataset, it is necessary to calculate objective indicators to assess whether the model has generated relevant predictions for the variable under study, such as the coefficient of determination $R^2$, whose formula is written:

$$R^2 = 1 - \frac{\sum_{i=1}^{n}(y_i - \hat{y}_i)^2}{\sum_{i=1}^{n}(y_i - \bar{y}_i)^2} \quad (7)$$

The Root Mean Square Error (RMSE) is considered an excellent general-purpose error measure for numerical predictions and the Mean Absolute Deviation (MAD) is a measure of variability that indicates the average distance between observations and their mean. These are written as follows:

$$RMSE = \sqrt{\frac{1}{n}\sum_{i=1}^{n}(y_i - \hat{y}_i)^2} \quad (8)$$

$$MAD = \frac{1}{n}\sum_{i=1}^{n}(y_i - \bar{y}_i)^2 \quad (9)$$

where:

$\hat{y}_i$ : Predicted response

$y_i$ : Experiment response

$\bar{y}_i$ : Average response.

The artificial neural network to optimize the regression models uses the $RMSE$ and $MAD$ metrics, which are expressed in the same unit as the variable being predicted and are therefore easier to interpret. These metrics quantify the errors made by the model. The higher they are, the worse the model performs.

## 3. RESULTS AND DISCUSSION

After carrying out the tests in accordance with Taguchi's L9 orthogonal, the wear W and roughness ($Ra, Rt$ and $Rz$) are measured, and the results are summarized in Table 4.

- $W$: wear $(mm)$;
- $Ra$: arithmetic mean deviation of the evaluated profile $(\mu m)$;
- $Rt$: sum of the greatest of the projection heights and the greatest of the depression depths $(\mu m)$;
- $Rz$: height of the maximum irregularities of the profile $(\mu m)$.

Table 4. Summary of inputs and outputs of the experiments conducted.

| **Tests** | $v\ (cSt)$ | $T\ (\mu m)$ | $Q\ (N)$ | $V(rpm)$ | $W(mm)$ | $Ra\ (\mu m)$ | $Rt\ (\mu m)$ | $Rz\ (\mu m)$ |
|---|---|---|---|---|---|---|---|---|
| 1 | 220 | 63 | 100 | 200 | 0,005 | 0,304 | 2,38 | 1,6 |
| 2 | 220 | 90 | 130 | 800 | 0,022 | 0,572 | 4,2 | 5,5 |
| 3 | 220 | 125 | 160 | 1600 | 0,034 | 0,69 | 7,4 | 10,3 |
| 4 | 150 | 63 | 130 | 1600 | 0,014 | 0,284 | 1,82 | 0,68 |
| 5 | 150 | 90 | 160 | 200 | 0,014 | 0,382 | 1,46 | 1,08 |
| 6 | 150 | 125 | 100 | 800 | 0,028 | 0,546 | 2,88 | 1,6 |
| 7 | 37 | 63 | 160 | 800 | 0,024 | 0,436 | 2,3 | 1,74 |
| 8 | 37 | 90 | 100 | 1600 | 0,018 | 0,464 | 2,22 | 1,96 |
| 9 | 37 | 125 | 130 | 200 | 0,016 | 0,442 | 2,16 | 1,34 |

4.1. Application of artificial neural network model

The prediction models obtained by our study are deemed acceptable with overall coefficients of determination close to 1:

- $R^2$ learning = 0.9990506
- $R^2$ validation = 0.9257915

Where:

$$W_1 = 0.5 * \begin{bmatrix} 0.022873 & -0.025525 & 0.027293 & -0.001924 \\ -0.00841 & 0.006122 & -0.015278 & -0.001428 \\ -0.02125 & 0.063339 & -0.013787 & -0.00032 \end{bmatrix}$$

$$b_1 = \begin{bmatrix} 5.3876555 \\ 3.680334 \\ -1.626522 \end{bmatrix}$$

$$W_2 = \begin{bmatrix} 0.000855 & -0.016442 & 0.014373 \\ 0.027237 & -0.205278 & 0.260805 \\ -0.720235 & -0.985626 & 1.739268 \\ -1.548099 & -1.407945 & 2.624222 \end{bmatrix}$$

$$b_2 = \begin{bmatrix} 0.019375 \\ 0.495760 \\ 3.252981 \\ 3.547100 \end{bmatrix}$$

$$y = \begin{bmatrix} W \\ Ra \\ Rt \\ Rz \end{bmatrix}$$

- **Validation of artificial neural network model**

The model validation parameters: $R^2$, RMSE and MAD, are deemed acceptable and their values are presented in Table 5.

This involves carrying out additional experiments at different points in the study area. When the measured values are compared with the model predictions, we see that test points a, b, and c are near the predicted points (Fig. 3). The coefficients of determination $R^2$ reported in Table 6 show an acceptable level of error for the model.

Effect of input parameters on responses.

The main effects correspond to the values of the weights W1i; if the values of the latter are significant, the corresponding inputs Xi are those that influence the output, values Yi. The average change in response from the low level of input Xi to its high level gives the total effect of a factor.

Using the grouped histograms of the main effects (Fig. 4) and the overall effects (Fig. 5), the following observations can be made:

- The summary of the overall ratio for the main effect clearly indicates that solid pollution has a dominant impact of 0.396, followed by viscosity in second place, with an effect equal to 0.243.

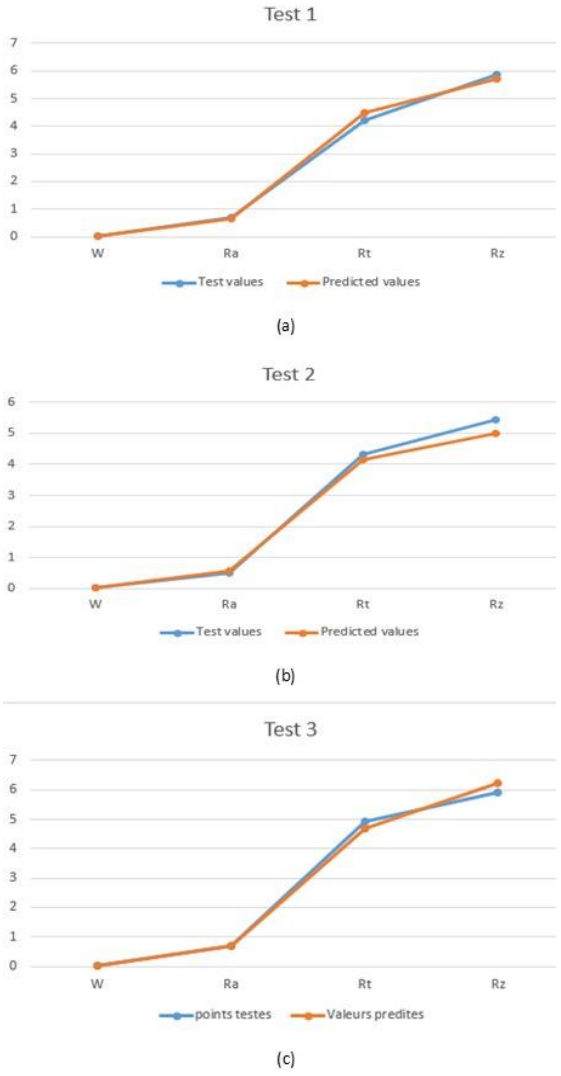


Fig. 3. Comparing experimental and predicted values

Table 5. Model validation parameters: $R^2$, $RMSE$ and $MAD$.

| Measures | | Value | |
|---|---|---|---|
| | | Training | Validation |
| $W\ (mm)$ | Determination coefficient $R^2$ | 0,65018 | 0,9206482 |
| | Root mean square error ($RMSE$) | 0,0044228 | 0,0025335 |
| | Mean absolute deviation ($MAD$) | 0,0037957 | 0,002371 |
| $Ra\ (\mu m)$ | Determination coefficient $R^2$ | 0,6880061 | 0,9650908 |
| | Root mean square error ($RMSE$) | 0,0611414 | 0,0249095 |
| | Mean absolute deviation ($MAD$) | 0,0415199 | 0,0221399 |
| $Rt\ (\mu m)$ | Determination coefficient $R^2$ | 0,9337517 | 0,5627107 |
| | Root mean square error ($RMSE$) | 0,197226 | 1,7527859 |
| | Mean absolute deviation ($MAD$) | 0,1560046 | 1,5285203 |
| $Rz\ (\mu m)$ | Determination coefficient $R^2$ | 0,7989301 | 0,6336219 |
| | Root mean square error ($RMSE$) | 0,689519 | 2,5945114 |
| | Mean absolute deviation ($MAD$) | 0,6375022 | 2,2354322 |

Table 6. Summary of wear and roughness validation testes

| values | ν (cSt) | T (µm) | Q (N) | V (rpm) | W | Ra | Rt | Rz |
|---|---|---|---|---|---|---|---|---|
| Predicted values | 40 | 90 | 140 | 400 | 0.021 | 0.567 | 4.156 | 5.006 |
| | 40 | 90 | 140 | 1600 | 0.029 | 0.672 | 4.502 | 5.73 |
| | 40 | 120 | 140 | 1000 | 0.03 | 0.7 | 4.7 | 6.21 |
| Test values | 40 | 90 | 140 | 400 | 0.021 | 0.567 | 4.156 | 5.006 |
| | 40 | 90 | 140 | 1600 | 0.029 | 0.672 | 4.502 | 5.73 |
| | 40 | 120 | 140 | 1000 | 0.03 | 0.7 | 4.7 | 6.21 |
| $R^2$ | | | | | 0.9960 | 0.9090 | 0.9860 | 0.7869 |

- It can also be observed that the summary of the overall ratio of the total effect indicates that solid pollution has the first impact, with a value of 0.462, followed by viscosity with an effect equal to 0.323. These two factors visibly contribute to the increase in wear and roughness $Ra, Rt$ and $Rz$, and may therefore cause the early degradation of the elastohydrodynamic contact studied.
- The wear and roughness $Ra$ are influenced first by the size of the pollutant$T$, followed in second place by the viscosity$\nu$; on the other hand, the latter affects first the variation of the roughness's $Rt$ and $Rz$.

We used the desirability function proposed by Derringer and Suich [26]. The overall desirability $D$ is the geometric mean of the individual desirability $d_i$. The desirability $D$ is determined by the formula:

$$D = \left(d_1, d_2 \dots, d_n\right)^{\frac{1}{n}}$$

Where:

$d_i (i = 1, 2, \dots, n)$ is the individual desirability.

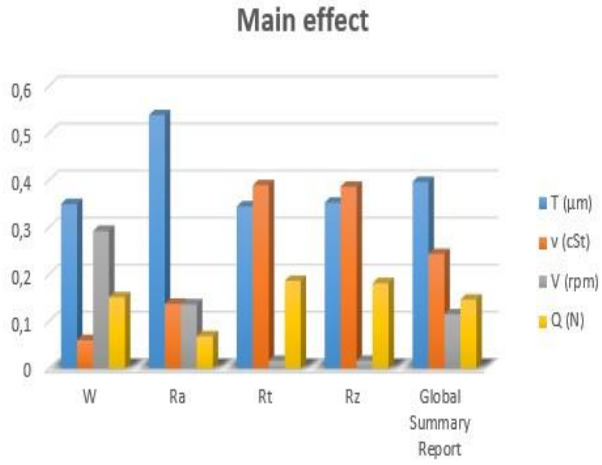


Fig. 4. Main effect of factors on wear W, roughness Ra, Rt, Rz and the global factor ratio

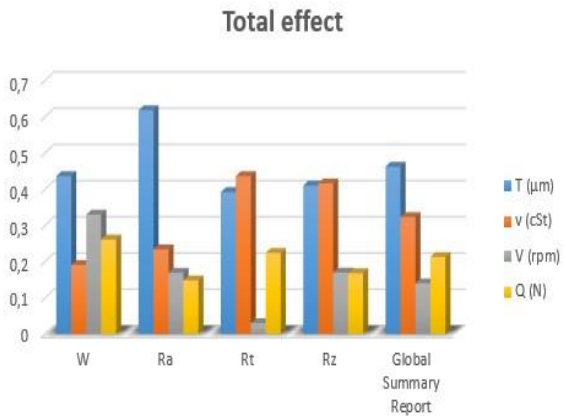


Fig. 5. Total effect of factors on wear W, roughness Ra, Rt, Rz and the global ratio of factors

The relationship between the predicted response of one or more dependent variables and the desirability of the response is called the desirability function. To define the desirability of a response, one must first specify a desirability function for each dependent variable, assigning scores from 0 (unfavorable) to 1 (very desirable) to the predicted values. The individual desirability $d_i$ of the predictors for each dependent variable is then summarised by calculating their geometric mean. The desirability profiles consist of a series of graphs, one for each independent variable, showing the overall desirability at different levels for an independent variable, while the other independent

variables do not change in level. By examining the desirability profile, we can visually determine the level of the predictor that produces the most desirable predictive response for the dependent variable.

The prediction profiler allowed a more detailed reading of the effects of the factors on wear W and roughness $Ra, Rt$ and $Rz$. This tool allows the optimisation of the operating environment by exploiting the effects of the most dominant parameters on the degradation. Fixing the speed at $1600\ rpm$ and the load at $160\ N$, we combined the maximum and minimum values of the kinematic viscosity υ and the grain size $T$. Using Figs. 6, 7, 8 and 9, we find that when the grain size $T = 63\ \mu m$, the values of wear W and roughness Ra are minimal ($W = 0.023\ mm$ and $Ra = 0.5\ \mu m$ (Fig. 8); $W = 0.026\ mm$ and $Ra = 0.26$ (Fig. 6)). On the other hand, the kinematic viscosity $\upsilon = 220\ cSt$ influences the variation of the terms $Rt$ and $Rz$, the latter taking minimal values ($Rt = 2.63\ \mu m$ and $Rz = 2.38$ (Fig. 6)).

The presence of large sand particles ($T = 125\ \mu m$) in the lubricant increases wear by abrasion of the surfaces in contact (Figs. 7 and 9). Thus, the unavoidable presence of solid particles in the lubricant has a double effect; on the one hand it accelerates the degradation of the surfaces in contact and on the other it leads to the degradation of the main physical–chemical properties of the lubricants. The results obtained show the reasons for the reduction in the life of elastohydrodynamic systems in a polluted environment.

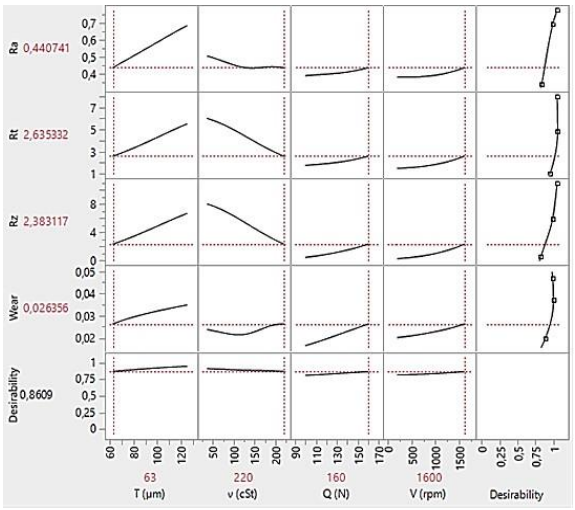


Fig. 6. Prediction of wear and roughness (Ra, Rt and Rz) for the parameters: υ = 220 cSt; V = 1600 rpm; T = 63 µm; Q = 160 N

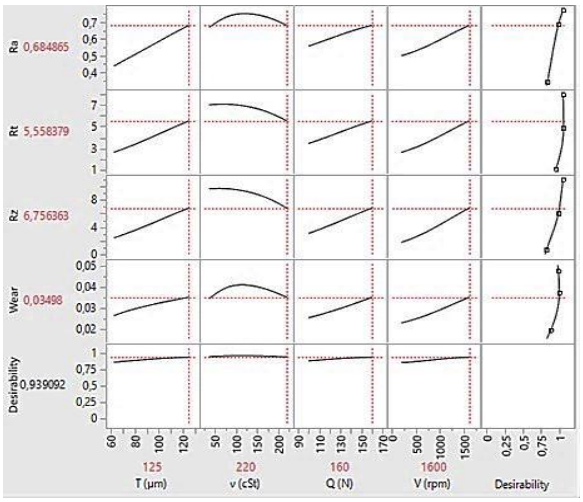


Fig. 7. Prediction of wear and roughness (Ra, Rt and Rz) for the parameters: υ = 220 cSt; V = 1600 rpm; T = 125 µm; Q = 160 N

According to the analysis carried out using the artificial neural network, it was found that pollution is the most influential parameter on the degradation of the elastohydrodynamic contact studied, but this dominance does not exclude the effect of the viscosity of the lubricant on the roughness measured.

A photo was taken at ×240 magnification, from which a change in the surface condition compared to the new condition (Fig. 10) and a different morphology can be seen. This is due to the variation of the four parameters simultaneously.

Firstly, Figs. 11, 15 and 19 show very deteriorated surfaces due to the low contact speed.

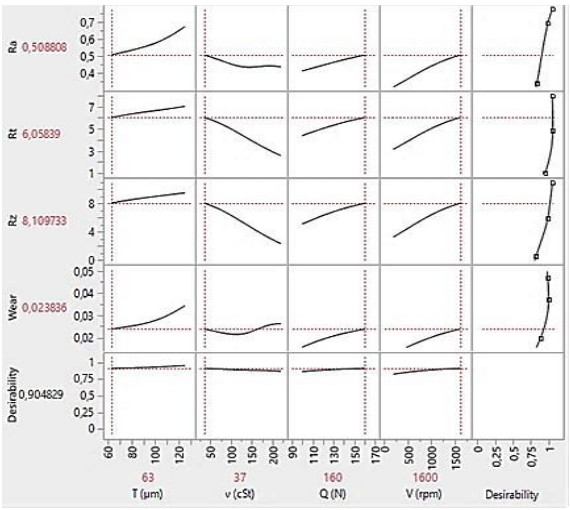


Fig. 8. Prediction of wear and roughness (Ra, Rt, and Rz) for the parameters: υ = 37 cSt; V = 1600 rpm; T = 63 µm; Q = 160 N

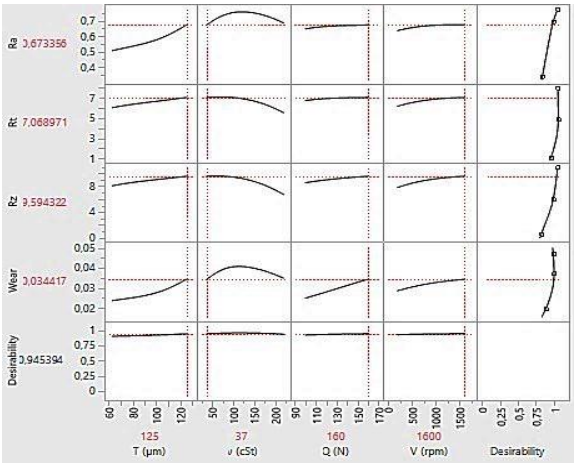


Fig. 9. Prediction of wear and roughness (Ra, Rt, and Rz) for the parameters: υ = 37 cSt; V = 1600 rpm; T = 125 µm; Q = 160 N

It should be noted that when the speed of the surfaces is low, the debris remains grouped and produces wider and deeper indentations. The indentations in themselves do not present a real danger for the surfaces or therefore for the parts in contact. However, the cyclic passage of this indent into the contact and the change in the pressure and stress field can lead to the formation of micro-cracks that can produce flaking [27]. The viscosity of the lubricant and the size of the grains are at the origin of the different morphology of the results obtained, the brittle particles explode at the entrance of the EHD contact, producing small fragments that result in a larger number of particles that indent the surfaces. Low viscosity does not allow good protection of the contacting surfaces, which can be underfed, and this is accentuated with contacts operating at low speeds. Underfeeding, which is caused by insufficient amounts of lubricant at the contact entrance, also increases the risk of damage. Indeed, it is well established that a reduction in the amount of lubricant available causes a decrease in the thickness of the separator film [28, 29].

Secondly, it is noted that tests 7 Fig. 17, 6 Fig. 16 and 2 Fig. 12 show less surface modification than tests 1 Fig. 11, 5 Fig. 15 and 9 Fig. 19, with a spacing between the craters produced by the indents. The contact operating at a rotation speed of 800 rpm induces a wider spalling, the image of test 7 ($\upsilon = 37\ cSt; T = 63\ \mu m$ and $Q = 160\ N$) shows quite a lot of spalling compared to test 6 and 2, and the low viscosity and higher load cause quite deep craters. In pure running condition, the particles do not embed themselves on the surface of the lubricated contacts. It should be noted that the presence of even a small amount of slip significantly alters the indentation pattern.

Moreover, the presence of sliding causes a scattering of debris, which induces greater damage to the surface, and it happens that particles remain embedded and pass several times in the contact [27]. This phenomenon is observed in test 8 Fig. 18, test 4 Fig. 14 and test 3 Fig. 13, as the sliding speed is more visible, (tests 3 Fig. 13 and test 4 Fig. 14) with a speed of 1600 rpm in the presence of solid pollution. Furthermore, lubrication with an oil of kinematic viscosity υ = 37 cSt accentuates the size of the craters and this is shown by the image of test 8 in Fig. 18.

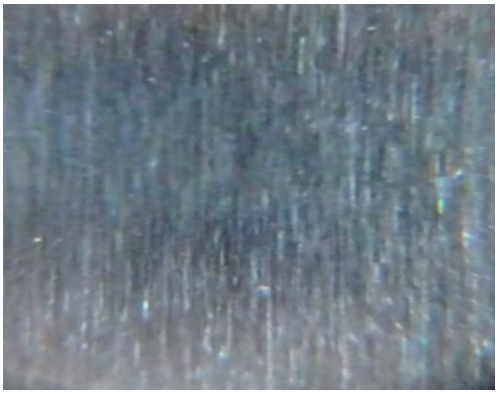

Fig. 10. Original state photo of the contact surfaces, magnification ×240 (specimen)

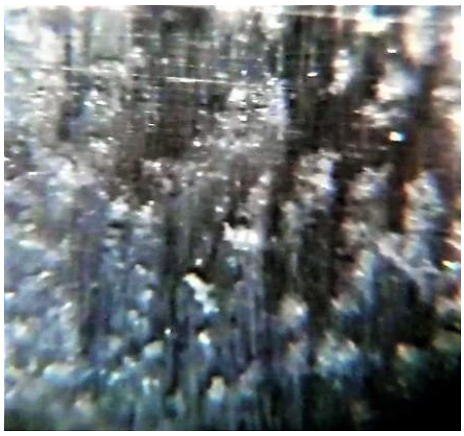

Fig. 11. Photo of the contact surfaces (magnification ×240). Test 1: =220 cSt; V=200 rpm; T=63 µm; Q= 100 N

Fig. 12. Photo of the contact surfaces (magnification ×240). Test 2: υ=220 cS; V=800 rpm; T=90 µm; Q= 130 N

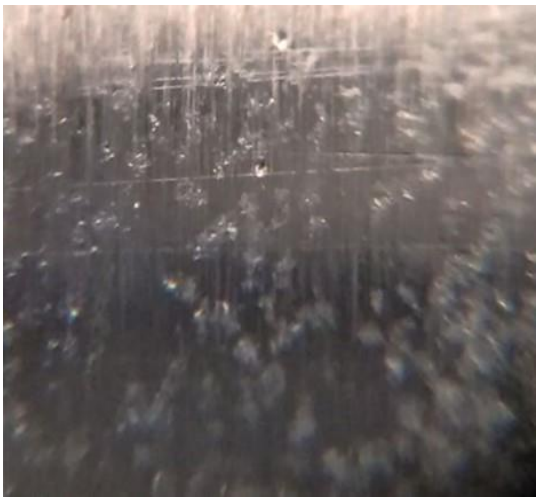

Fig. 13. Photo of the contact surfaces (magnification ×240). Test 3: =220 cSt; V=1600 rpm; T=125 µm; Q= 160 N

Fig. 14. Photo of the contact surfaces (magnification ×240). Test 4: =150 cSt; V=1600 rpm; T=63 µm; Q= 130 N

Fig. 15. Photo of the contact surfaces (magnification ×240). Test 5: =150 cSt; V=200 rpm; T=90 µm; Q= 160 N

Fig. 16. Photo of the contact surfaces (magnification ×240). Test 6 : =150 cSt ; V=800 rpm ; T=125 µm ; Q= 100 N. N

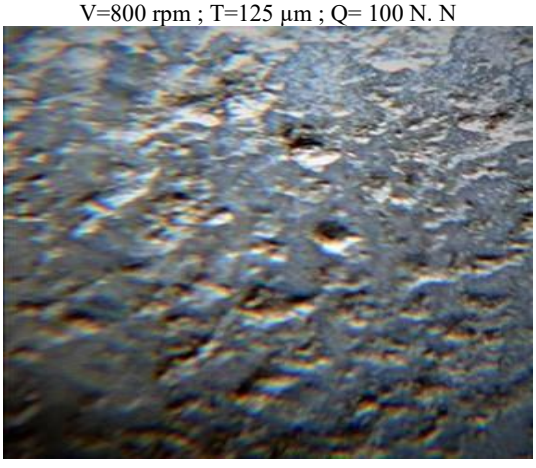

Fig. 17. Photo of the contact surfaces (magnification ×240). Test 7: υ=37 cSt; V=800 rpm; T=63 µm; Q= 160 N

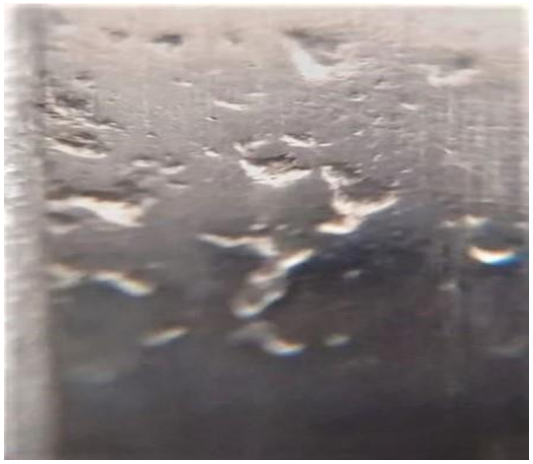

Fig. 18. Photo of the contact surfaces (magnification ×240). Test 8: υ=37 cSt; V=1600 rpm; T=90 µm; Q= 100 N

Fig. 19. Photo of the contact surfaces (magnification ×240). Test 9: =37 cSt; V=200 rpm; T=125 µm; Q= 130 N.

## 5. CONCLUSIONS AND FUTURE WORK

Elastohydrodynamic contacts are a mysterious field of research, where several phenomena occur. The operating environment and their interactions give rise to complex behaviours that are difficult to explain. In this paper we have tried to give answers by using a Taguchi L9 design of experiment, which allowed us to combine four parameters: rotation speed $V$, load $Q$, kinematic viscosity $\upsilon$ and solid pollutant (sand) $T$. The processing of the results is carried out using an artificial neural network to identify the parameters that have an impact on the degradation in terms of wear $W$ (loss of dimension) and surface condition by the indicators: $Ra, Rt$ and $Rz$.

- This approach allowed us to:
- Write prediction models for wear and roughness $Ra, Rt$ and $Rz$ with global determination coefficients close to 1: $R^2$ learning = 0.9985 and $R^2$ validation = 0.9996.
- To predict with the desirability function the minimum degradation of the elastohydrodynamic contact studied, for which wear of 0.026 mm and roughness's $Ra = 0.44\ \mu m, Rt = 2.63\ \mu m$ and $Rz = 2.38\ \mu m$ are predicted, under the effect of the operating environment : $\upsilon = 220\ cSt$; $V = 1600\ rpm$; $T = 63\ \mu m$; $Q = 160\ N$.
- On the other hand, we concluded that the presence of large solid contaminants leads to accelerated surface degradation. Furthermore, mechanical contacts operating with high viscosity lubricants are less deteriorated than those using low viscosity lubricants.
- Speed and load in turn influence contact deterioration; and their effect is visible in the quality of the contacting surfaces, such as indentation and spalling.
- Indentation of the surfaces leads to disruption of the oil film, and thus accelerates the degradation process.

As future work, we plan to study the variation of the low viscosity lubricant film as a function of metal debris from the operation of the elastohydrodynamic contact with a new approach.

**Source of funding:** *This research received no external funding.*

**Author contributions:** *research concept and design, S.M..; Collection and/or assembly of data, S.M.; Data analysis and interpretation, S.M., R.K., H.LM., A.K..; Writing the article, S.M., R.K.; Critical revision of the article, S.M., R. K., H.LM., A.K.; Final approval of the article, S.M., R.K., H.LM., A.K.*

**Declaration of competing interest:** *The authors declare that they have no known competing financial interests or personal relationships that could have appeared to influence the work reported in this paper.*

## REFERENCES

1. Zhu D, Wang QJ. EHL History (Elastohydrodynamic Lubrication). Encyclopedia of Tribology 2013 s. 832–47. https://doi.org/10.1007/978-0-387-92897-5_625.
2. Lugt PM, Morales-Espejel GE. A Review of Elasto-Hydrodynamic Lubrication Theory. Tribology Transactions 2011; 54(3): 470–96. https://doi.org/10.1080/10402004.2010.551804.
3. Krupka I, Sperka P, Hartl M. Effect of surface roughness on lubricant film breakdown and transition from EHL to mixed lubrication. Tribology International 2016; 100: 116–25. https://doi.org/10.1016/j.triboint.2015.12.008.
4. Guegan J, Kadiric A, Spikes H. A Study of the Lubrication of EHL Point Contact in the Presence of Longitudinal Roughness. Tribology Letters 2015; 59(1): 22. https://doi.org/10.1007/s11249-015-0549-7.
5. Azman SSN, Zulkifli NWM, Masjuki H, Gulzar M, Zahid R. Study of tribological properties of lubricating oil blend added with graphene nanoplatelets. Journal of Materials Research 2016; 31(13): 1932–8. https://doi.org/10.1557/jmr.2016.24.
6. Senatore A, D'Agostino V, Petrone V, Sarno M, Ciambelli P. Graphene oxide nanosheets as effective

friction modifier for oil lubricant: Materials, methods, and tribological results. International Scholarly Research Notices 2013; e425809. https://doi.org/10.5402/2013/425809.
7. Ryniewicz AM, Bojko Ł, Madej T. The estimation of lubricity and viscosity of engine oils. Diagnostyka 2014;15(1):61–66
8. Jakubek B, Barczewski R. The influence of kinematic viscosity of a lubricant on broadband rolling bearing vibrations in amplitude terms. Diagnostyka 2018; 20(1): 93–102. https://doi.org/10.29354/diag/100440.
9. Roelands CJA. Correlational aspects of the viscosity-temperature-pressure relationship of lubricating oils. Journal of Lubrication Technology 1966; 93(1), p209. http://resolver.tudelft.nl/uuid:1fb56839-9589-4ffb-98aa-4a20968d1f90
10. Dwyer-Joyce RS, Reddyhoff T, Zhu J. Ultrasonic measurement for film thickness and solid contact in elastohydrodynamic lubrication. Journal of Tribology 2011; 133(031501). https://doi.org/10.1115/1.4004105.
11. Chen K, Zeng L, Chen J, Ding X. Analysis of line contact elastohydrodynamic lubrication with the particles under rough contact surface. Advances in Materials Science and Engineering 2020; 2020: e5420426. https://doi.org/10.1155/2020/5420426.
12. Shengguang Z, Wenzhong W, Ziqiang Z. Elastohydrodynamic Lubrication Analysis of Point Contacts With Consideration of Material Inhomogeneity. Journal of Tribology 2014; 136(041501). https://doi.org/10.1115/1.4027750.
13. Wang Z, Han B, Sun L. Analysis of Elastohydrodynamic Lubrication (EHL) Characteristics of Port Plate Pair of a Piston Pump. Machines 2022; 10(12): 1109. https://doi.org/10.3390/machines10121109.
14. Patir N, Cheng HS. An average flow model for determining effects of three-dimensional roughness on partial hydrodynamic lubrication. Journal of Lubrication Technology 1978; 100(1): 12–17.
15. Krupka I, Sperka P, Hartl M. Effect of surface roughness on lubricant film breakdown and transition from EHL to mixed lubrication. Tribology International 2016. 100: 116–125.
16. Zapletal T, Sperka P, Krupka I, Hartl M. The effect of surface roughness on friction and film thickness in transition from EHL to mixed lubrication. Tribology International 2018; 128: 356–64. https://doi.org/10.1016/j.triboint.2018.07.047.
17. Morales-Espejel GE. Surface roughness effects in elastohydrodynamic lubrication: A review with contributions. Proceedings of the Institution of Mechanical Engineers, Part J: Journal of Engineering Tribology 2014; 228(11): 1217–42. https://doi.org/10.1177/1350650113513572.
18. Greenwood JA, Morales-Espejel GE. The behaviour of transverse roughness in EHL contacts. Proceedings of the Institution of Mechanical Engineers 1994; 208: 121–132.
19. Hansen J, Björling M, Larsson R. A New film parameter for rough surface EHL contacts with anisotropic and isotropic structures. Tribology Letters 2021; 69(2): 37. https://doi.org/10.1007/s11249-021-01411-3.
20. Bonetto A, Nélias D, Chaise T, Zamponi LA. Coupled euler-lagrange model for more realistic simulation of debris denting in rolling element bearings. Tribology Transactions 2019; 62(5): 760-778.
21. George K Nikas. Particle entrapment in elliptical, elastohydrodynamic, rough contacts and the influence of intermolecular (van der Waals) forces. Proceedings of the Institution of Mechanical Engineers, Part J: Journal of Engineering Tribology 2021; 235(11): 2227-2246.
22. Sui T, Song B, Zhang F, Chen Y, Yan S, Wang A, Ding M. The flow characteristics of solid particles used as additives for lubricants in the point contact area. RSC Advances 2018; 8(17): 9457-9461.
23. Strubel V, Simoens S, Vergne P, Fillot N, Ville F, El Hajem M, Devaux N, Mondelin A, Maheo Y. Fluorescence tracking and μ-PIV of individual particles and lubricant flow in and around lubricated point contacts. Tribology Letters 2017; 65: 3.
24. Sari MR, Maatallah S, Adjabi R, Khochemane L. Experimental and statistical investigation on the failure of contaminated elastohydrodynamic lubrication rolling contact. Proceedings of the Institution of Mechanical Engineers, Part J: Journal of Engineering Tribology 2016; 230(3): 300–22. https://doi.org/10.1177/1350650115600738.
25. Maatallah S, Sari MR, Khochemane L. Effect of Lubricant Contamination on EHL Rolling Contact: Response Surface Methodology. Transactions d'ingénierie 2016; 64(1): 69-88. www.entra.put.poznan.pl/index.php/et/article/view/270/249.
26. Derringer D, Suich R. Simultaneous optimisation of several response variables. Journal of Quality Technology 1980; 12: 214-219.
27. Fabrice Ville. Pollution solide des lubrifiants, indentation et fatigue des surfaces. Sciences de l'ingénieur. INSA de Lyon 1998.
28. Chevalier F, Lubrecht AA, Cann PME, Colin F, Dalmaz G. Film thickness in starved EHL point contacts. Journal of Tribology 1998; 120(1): 126-133.
29. Damiens B, Venner CH, Cann PME, Lubrecht, AA. Starved lubrication of elliptical EHD contacts. Journal of Tribology 2004; 126(1): 105-111.

**Sabrina MATTALLAH**
Received the Magister degree in Mechatronics, Construction Mechanics in 2011. Ph.D. degree in Mechatronics, Electromechanics in 2016. His current position is Full Lecturer at the University 20 August 1955 of Skikda. His research interests are oriented towards Tribology, and applications of statistical modelling and artificial intelligence.
e-mail: s.mattallah@univ-skikda.dz

**Hanane LOUAHEM M'SABAH**
Received the diploma of Ph.D. degree in Electromechanics, Industrial Mechanization in 2016. His current position is a full Lecturer at the University 20 August 1955 of Skikda. His research interests are oriented towards maintenance, forecasting model, statistical methods, and stochastic process.
e-mail: louahem.hanen@gmail.com

**Ridha KELAIAIA**
Received the diploma of magister in Robotics, Automation and Industrial Data Processing and Ph.D. degree in 2012. His current position is a full professor at the University of Skikda. His research interests are oriented towards Robotics, Electromechanics and Engineering Applications of Artificial Intelligence.
e-mail: r.kelaiaia@univ-skikda.dz

**Adlen KERBOUA**
Received his MSc (2004) and magister (2012) in computer sciences, PhD (2018). Currently, he is associate professor in the University of Skikda, Algeria. His current research is oriented toward neural network and artificial intelligence. e-mail: ad.kerboua@univ-skikda.dz